Hindawi Publishing Corporation
Journal of Applied Mathematics
Volume 2015, Article ID 283843, 7 pages
http://dx.doi.org/10.1155/2015/283843

Research Article

Finite Element Simulation of the Compaction and Springback of Alumix 321 PM Alloy

Stanley G. Selig and Darrel A. Doman

Department of Mechanical Engineering, Dalhousie University, 1360 Barrington Street, P.O. Box 15000, Halifax, NS, Canada B3H 4R2

Correspondence should be addressed to Darrel A. Doman; darrel.doman@dal.ca

Received 29 April 2015; Revised 3 July 2015; Accepted 15 July 2015

Academic Editor: Sutasn Thipprakmas

A finite element simulation of the compaction and springback of an aluminum-based powder metallurgy alloy (Alumix 321) was developed and validated using the LS-DYNA hydrocode. The present work aims to directly address the current scarcity of modeling works on this popular alloy system. The Alumix 321 constitutive material parameters are presented. The model can predict the results of single-action compaction as well as the amount of springback experienced by a compact upon ejection from the die. The model has been validated using a series of experiments including powder compaction, optical densitometry, and the creation of a compaction curve.

1. Introduction

Powder compaction is a critical step in the powder metallurgy (PM) process since the overall performance of a PM part is largely based on the quality of the compaction. The quality of a compact can be quantified by the densification of the part, where the focus is on the distribution of the local densities. Strength and other material properties increase with density, so it is important that the part is both dense and uniform after the compaction step. If there are large variations in the density found throughout a part, low-density areas will be weak points in the compact and will lead to reduced overall part quality [1].

Aluminum powder metallurgy (Al PM) is a fast-growing segment of the PM industry as automotive manufacturers look to reduce the overall weight of vehicles by replacing a range of ferrous PM components and thus increase their fuel efficiency. PM aluminums are looked to as feasible substitutes in the place of both die-cast aluminum and iron PM materials for moving engine components. As strength and other material properties increase with density, the reliability of PM parts is affected by both the bulk density and density gradients within the green compacts. Similarly, the dimensional tolerance of the final compact is affected by warping during sintering as well as the elastic springback experienced by the green compact upon ejection from the die [1]. It is for these reasons that this work investigates the density distribution and springback found within PM parts. Due to its attractive engineering qualities Al PM research is expanding, with recent works focusing on as-made mechanical properties [2] and sintering responses [3].

There are many phenomena that occur during the compaction process that deal with the mechanics of powder compaction, and therefore research has focused on several particular aspects of the process. Some of the major areas of research in terms of powder compaction phenomena include die wall friction and the effects of lubrication (admixed and sprayed on die wall) on the final state of the compact [4–8], accurately modelling metal powder behaviour in terms of the densification mechanics during compaction [4, 9, 10]. These phenomena are often difficult to measure experimentally, but finite element (FE) analysis can provide researchers with detailed information: forces at the die-powder interface, internal plastic strains, pressure transmission through the powder, and others.

This work first presents the experimental setups and numerical models used to investigate the compaction and springback of an aluminum-based PM powder (ECKA Granules' Alumix 321). It is noted that while there has been considerable research focus on the postcompaction processing

Table 1: Properties of ECKA Alumix 321 powder (ECKA Granules, 2012).

Alloy	Mg %	Si %	Cu %	Microwax C (lubricant)	Al %
AlMgSiCu	1	0.5	0.2	1.5	Remainder

of Al PM alloys, few works have been carried out on the FE modeling of the compaction and springback processes and more specifically Alumix 321. Results of each will be shown and compared, and conclusions will be drawn about the results of the numerical and experimental work.

2. Experimental Methods

In order to validate the compaction model, a number of experiments were performed on powder compacts. The experimental methods used can be divided into two major categories: powder characterization and powder consolidation. Powder characterization consists of three experiments: constructing a compaction curve, determining the flow rate of the powder, and determining the apparent density of the powder prior to compaction. The powder consolidation category consists of powder compaction and optical densitometry. Optical densitometry is a method of mapping the density distribution within the powder compact using microscopy and photo analysis. The material composition of the Alumix 321 powder used is shown in Table 1.

2.1. Powder Characterization. Several experiments have been performed to characterize the powder based on its attributes. These include creating a compaction curve based on the MPIF (Metal Powder Industries Federation) Standard 45, determining the flow rate of a powder following MPIF Standard 03 and determining the apparent density of the powder following MPIF Standard 48.

Three samples each were pressed in 100 MPa increments from 100 MPa to 500 MPa in a single-action compaction configuration. The material used in this powder characterization test has a lubricant premixed in the powder and no additional lubrication was employed during compaction. The sample heights were measured using a 0.001 mm precision micrometer. The diameter of each was measured using the same micrometer at the top, middle, and bottom of each sample, and the average of each was calculated. The samples were weighed to the nearest 0.01 g. The density of the test specimen was determined as

$$D = 1273\frac{M}{d^2h}, \tag{1}$$

where D = green density in g/cm^3, M = mass of test cylinder in g, d = diameter of test cylinder in mm, and h = height of test cylinder in mm.

This test utilizes a Hall Flowmeter Funnel having a calibrated orifice of 2.54 mm diameter. As per MPIF Standard 03, 50.0 g of powder is measured out into a clean weighing dish. The powder is then passed through the funnel and the elapsed time is recorded to the nearest 0.1 s. The flow rate of this Alumix 321 powder had an average measured flow rate of 17.5 s/50 g.

The apparent density of powder was measured as per the MPIF Standard 48. The Arnold apparent density, ρ_A, is calculated as

$$\rho_A = \frac{m}{V} = \frac{m}{20}, \tag{2}$$

where ρ_A is the Arnold apparent density in g/cm^3, m is the mass of the powder in g, and V is the volume of centre hole, which is 20 cm^3. The average Arnold apparent density for Alumix 321 powder was measured as 1.15 g/cm^3.

2.2. Powder Consolidation. The die compaction is carried out on a load-controlled 1 MN hydraulic press. The die used in this compaction is a single-action cylindrical die with a maximum rating of 600 MPa, a stationary lower punch and a floating upper punch. A load cell can be inserted between the upper punch and the top platen to get a reading of the upper punch force using a portable data acquisition system. Three tests were performed at each pressure and the sample height of each sample was measured before and after pressing.

After pressing, the samples were mounted in resin and ground to the bisecting plane of the cylinder using 240-grit sandpaper. Each sample was then ground using a 400-grit sandpaper until a relatively uniform surface with no large scratches was observed. This was followed by polishing using a 0.3 μm alumina suspension on a felt wheel for several minutes and a solution of 0.05 μm colloidal silica on a microcloth wheel by hand for several minutes. The densitometry analysis is performed using an optical microscope at 50x magnification with an Olympus digital camera equipped for data acquisition. Half of the cylinder was photographed and analyzed, as the sample is assumed to be axisymmetric and thus the two halves should be mirror images of one another.

The cylinder was mapped systematically beginning with the top outside corner. Images were collected manually by adjusting the microscope stage to capture contiguous images. An image of approximately 1.78 × 2.37 mm was captured using the software package ImagePro by Media Cybernetics. Once a column was completed, the stage was reset to the top and moved sideways in the same manner as just described. This was repeated such that the collected images represented half of the sample, as the sample is axisymmetric about the core axis. The images that are gathered are 8-bit greyscale: white representing the presence of aluminum and black representing pores in the microstructure; an example of which is shown in Figure 1.

Three samples were processed following the procedure previously described [11]: one at each of 100, 300, and 500 MPa compaction pressures. Shown in Figure 2 are the results for the density distribution contours for the 100, 300, and 500 MPa samples, respectively. The density contour maps reveal several important findings. The density contours in all three cases show a tendency to have higher density near the top half of the sample. This is where the greatest amount of powder flow is accumulating due to friction in the die

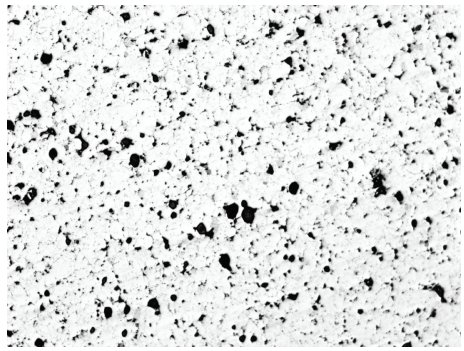

Figure 1: Micrograph taken of 300 MPa sample (50x magnification).

wall and where the highest density is expected to be seen. In particular, the density contour for 100 MPa shows the area of lowest density to be in the bottom outer ring, which is an expected result when comparing to the literature [1]. For the 300 MPa and 500 MPa samples, the highest density is found to be in the top outside ring, which is also a result which is expected as it is found in the literature. Furthermore, it is seen that the greatest disparity between highest and lowest density in a sample is found in the most lightly-compacted sample (85% to 63%) while the two samples compacted at higher pressure are much more uniform in density, ranging only about 2% from highest to lowest.

3. Finite Element Model

3.1. Model Geometry and Mesh. The geometry of the punches, die, and powder was constructed and meshed into discrete elements using Altair Hyperworks. The powder compaction was simulated in the time domain using the LS-DYNA hydrocode employing nonlinear material model formulations. The punches and die are assumed to be rigid bodies made of steel, and the powder is modelled using axisymmetric quadrilateral elements. The cylindrical die has a 15 mm diameter, and the initial fill height of the powder is 46.87 mm as determined by experimental measurement, which results in the powder being represented by 1410 elements.

3.2. Boundary Conditions and Loading. The lower punch and die wall are both fixed in both the axial and radial directions, while the upper punch is fixed in the radial direction but is free to move axially. The upper punch has a loading curve applied to mimicking the hydraulic press. The contact between the die wall, punches, and powder is modelled using a surface-to-surface contact algorithm in LS-DYNA and employs a Coulomb-type friction with a value of 0.24 that was taken from literature [9]. Standard LS-DYNA hourglass control has been used in this model, with the default coefficient of 0.10. This is implemented to help control possible instabilities that are sometimes encountered when running models.

3.3. Material Model and Parameter Determination. The Alumix 321 powder was modelled using the *MAT_GEOLOGIC_CAP_MODEL keyword [12], which is a representation of the Drucker-Prager Cap model. The parameters used to describe the material model were derived from the experimental triaxial data presented by Lee and Kim [9] and are presented in Table 2. The values here represent a prealloyed Al6061 powder supplied by Valimet used by Lee and Kim and will be the starting point to determine the parameters of the powder used in the experimental section of this work which is ECKA Alumix 321.

Table 2: Compaction material model parameters for Al6061 powder.

Parameter	Units	Value
Initial density	kg/m^3	1377
Initial bulk modulus	GPa	55.76
Initial shear modulus	GPa	13.26
Failure envelope parameter, Alpha	Pa	0
Failure envelope linear coefficient, Theta	—	0.394
Failure envelope exponential coefficient, Gamma	Pa	0 Pa
Failure envelope exponent, Beta	Pa^{-1}	0 Pa^{-1}
Cap surface axis ratio, R	—	2.800
Hardening law exponent, D	—	$5E-10$
Hardening law coefficient, W	—	0.62

3.4. Lee and Kim Validation. To validate the predicted densification of the Lee and Kim's model a model was constructed with the identical geometry of the die. This die is 20 mm in diameter and used an initial powder height of 30.05 mm. The simulation was run with the initial parameters derived from Lee and Kim's paper, and a parametric study was undertaken with the hardening law exponent, D, and the hardening law coefficient, W, to fit the model to results shown in Lee and Kim's paper. The values shown in Table 2 give a result that qualitatively matches the density distribution shape from the Lee and Kim Drucker-Prager Cap result (see Figure 3), with relative density values that are within 2% of those in Lee and Kim's paper; these results have a very good correlation given typical results in the literature.

3.5. Springback Model. Once the compaction model has reached completion, LS-DYNA models the springback of the compact after ejection from the die. The state of stress of each element is initialized in the solver, and the solver uses this as the input to calculate the eventual equilibrium of the system after elastic springback has taken place. As springback is essentially the release of elastic strain in the model, the DPC model is replaced by an elastic constitutive material model for this simulation. The density used for the springback model is the final density of the compaction simulation, and the Young's Modulus for the model is approximated as being the value of fully dense Al6061 multiplied by the relative density [13] and Poisson's ratio is assumed to be $\nu = 0.30$. These parameters will be used as a starting point for the determination of the model parameters for the Alumix 321 powder.

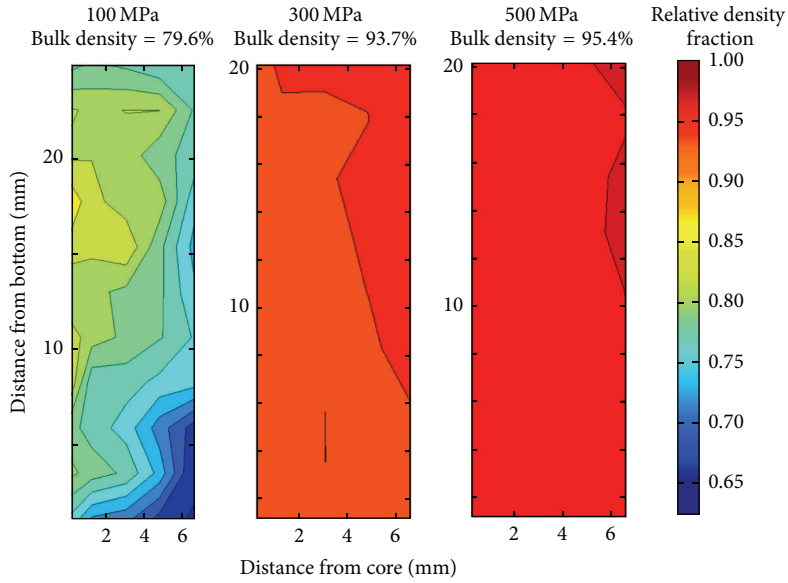

Figure 2: Relative density contour plots for 100, 300, and 500 MPa single-action samples.

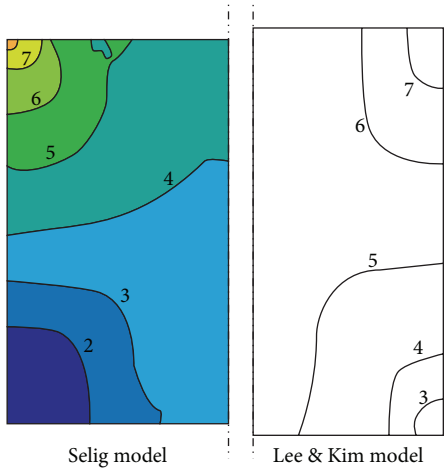

Figure 3: Comparison of model to Lee and Kim [9].

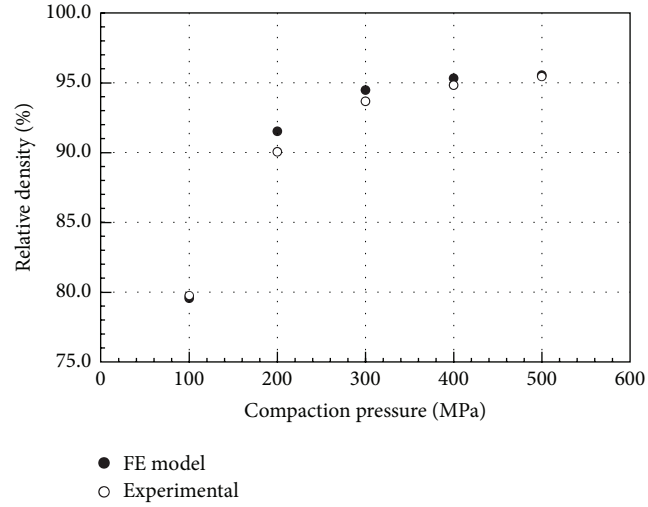

Figure 4: Comparison of relative bulk density from FE simulation to experimental data.

4. Results

4.1. Comparison of Model Results: Compaction Curve. In order to develop appropriate parameters for the Alumix 321 powder, the simulation results were compared to the experimental results. The initial relative density of the Alumix 321 powder in the die was calculated using the height of the powder column in the die, and the initial bulk and shear modulus were estimated to be those values corresponding to wrought Al6061 multiplied by the initial relative density. A parametric study with the D and W parameters was conducted to attempt to match the bulk density of the finite element sample at each compaction pressure to the experimental samples. LS-DYNA calculates the effective plastic strain, $\varepsilon_V^{\text{pl}}$, within each element, which is then converted to relative density, ρ_{rel}, through the relationship [10]:

$$\varepsilon_V^{\text{pl}} = \ln\left(\frac{\rho_{\text{rel},f}}{\rho_{\text{rel},0}}\right). \tag{3}$$

The bulk density was calculated by averaging the effective plastic strain over all the elements in the powder and converting it to relative density, where the resulting compaction curve is shown in Figure 4.

The resulting compaction curve using these parameters shows an excellent agreement between simulation data and

Table 3: Final compaction material model parameters for Al6061 powder.

Parameter	Units	Value
Initial density	kg/m^3	1207
Initial bulk modulus	GPa	48.87
Initial shear modulus	GPa	11.62
Failure envelope parameter, Alpha	Pa	0
Failure envelope linear coefficient, Theta	—	0.394
Failure envelope exponential coefficient, Gamma	Pa	0
Failure envelope exponent, Beta	Pa^{-1}	0
Cap surface axis ratio, R	—	2.800
Hardening law exponent, D	—	$1.4E-9$
Hardening law coefficient, W	—	0.76

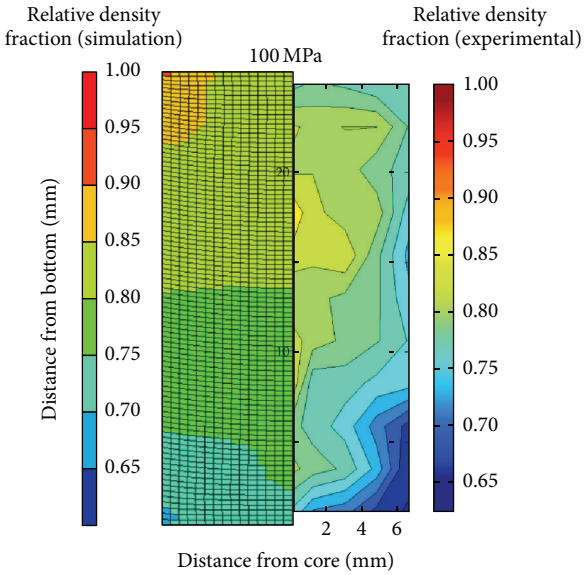

Figure 5: Comparison of density contour maps from experiment and finite element simulation (100 MPa).

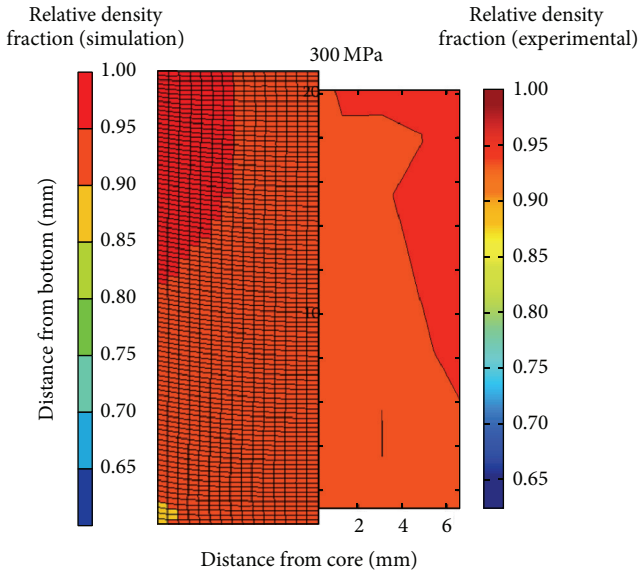

Figure 6: Comparison of density contour maps from experiment and finite element simulation (300 MPa).

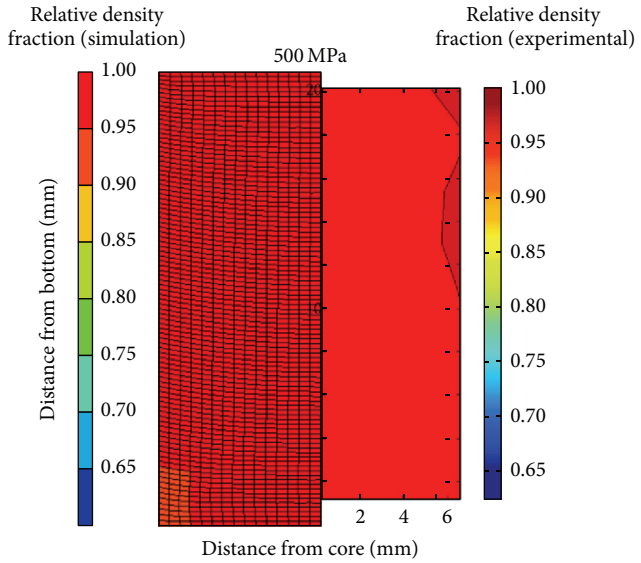

Figure 7: Comparison of density contour maps from experiment and finite element simulation (500 MPa).

experiment at the lowest compaction pressure, 100 MPa, and at the highest compaction pressure, 500 MPa. The values in-between are slightly overestimated using the finite element simulation but are considered a very good match. The DPC for Alumix 321 parameters are shown in Table 3.

4.2. Comparison of Model Results: Density Distributions. The density distribution within powder compacts at each pressure was investigated. As mentioned in the previous section, LS-DYNA calculates the effective plastic strain for each element; this value is then converted into percent relative density. Figures 5–7 show the deformed sample and the density distribution within the compact at 100, 300, and 500 MPa. For the 100 MPa sample, the element with the highest density is 90.4% and with the lowest density is 67.0%. For the 300 MPa sample, the highest density is 95.6% and lowest is 86.1%. For the 500 MPa sample, the highest density is 95.6% and lowest is 90.6%. In all cases, the density distribution qualitatively agrees with the predicted trend for density contours in a single-action die compaction [1], where the highest density occurs in the top outer ring of the powder compact, while the lowest density occurs in the bottom outer ring. Furthermore, the difference between the highest density and lowest density is greatest when the compaction pressure is low (23.4% range at 100 MPa), and this difference becomes very small as compaction pressure is increased (5% range at 500 MPa).

The information that can be extracted from the optical densitometry density distribution contour maps can be directly compared to the information taken from those created from the finite element simulations. Figures 5–7

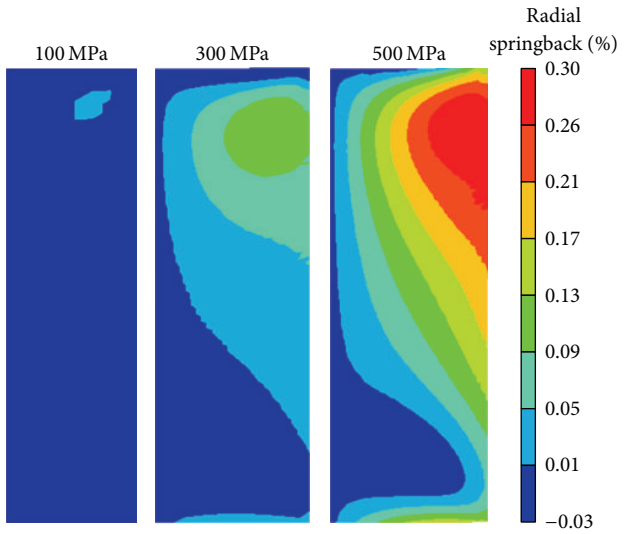

Figure 8: Radial springback of compact at 100, 300, and 500 MPa.

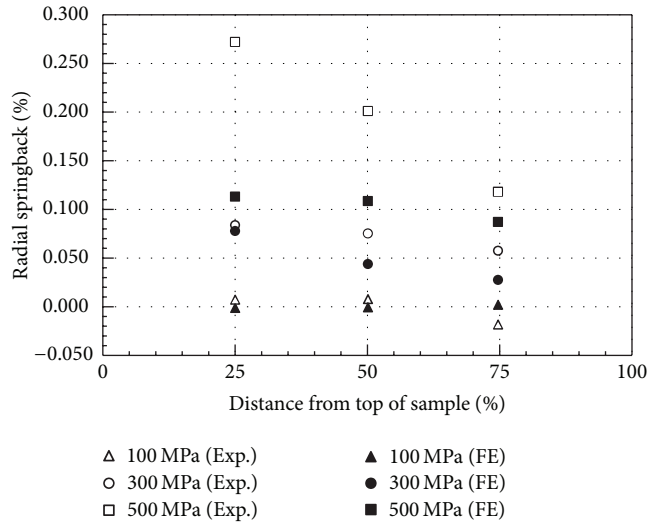

Figure 9: Comparison of radial springback from experiment and finite element simulation.

show the density distributions for 100, 300, and 500 MPa, respectively, for the optical densitometry experiments and the finite element simulations. Since the threshold value for the optical densitometry analysis was set so that the bulk density matched that of the physical compaction curve data, the contours can be compared directly between the densitometry and FE simulation data. The apparent size difference in the images is attributed to the fact that the optical densitometry contour maps are bound by the centroids of the outermost data points, which excludes approximately 1 mm off the external borders.

Though the contours are not identical, the trends found between the densitometry and finite element simulations are qualitatively very similar. The greatest difference between high and low density regions in a single compact is shown to be in the 100 MPa case in both the experimental data and simulation, and the uniformity in density increases as the compaction pressure is increased in both cases. In both instances as well, the highest density region is toward the top of the sample, whereas the lowest density region is toward the bottom of the sample. From this data, it shows that the two methods of analyzing the density contours in an Alumix 321 green sample are similar to one another and acceptable representations of this information.

4.3. Springback Model Results. The springback of the model at 100, 300, and 500 MPa was determined from the elastic springback model. Figure 8 shows a contour plot of radial displacement of the equilibrated compact after the springback simulation takes place for compaction pressures of 100, 300, and 500 MPa.

The fringe values in Figure 8 illustrate several of the fundamental mechanics of springback. The radial displacement values are very close to zero along the core, and the compact experiences an overall radial expansion; both of these responses are to be expected. Twisting of the compact is apparent: a nonconstant densification should lead to differing amounts of springback, as density is related to strength, which is related to residual stress, which ultimately controls springback.

Evaluating the percent dimensional change at several points along the height of the compact shows that the dimensional change is closely related to the relative bulk density at each area within the compact. Figure 9 gives a comparison of the experimental and simulated values of radial springback at 3 locations (25%, 50%, and 75% from the top of the compact) for three compaction pressures. The springback increases with both compaction pressure and local bulk density. These values are on the same order of the springback experienced by compacts upon ejection from a die in the literature [1, 13] where typical values range from 0.2% to 0.4%.

The diameters of the PM green compacts at each compaction pressure were measured at the top, middle, and bottom of the sample. These were converted into percent radial expansion and graphed in Figure 9 alongside the percent radial expansion calculated from the finite element springback model.

From this comparison, it is evident that both the experiment and finite element simulation show similar trends: the radial springback decreases from the top of the sample to the bottom of the sample and the radial springback increases overall with increasing compaction pressure. The results for both methods at 100 and 300 MPa show results that are very comparable with one another. The results at 500 MPa show larger springback in the simulation when compared to the experimental measurements, and this difference is much more evident near the top of the sample. Therefore, the springback model is better at predicting the springback of a compact at pressures of 300 MPa or less in its current state. It is hypothesized that the lack of modeling the compact ejection contributes to the overestimated springback due to overly high residual stresses.

5. Conclusions

FE model of the simulation of the compaction and springback of Alumix 321 PM alloy powder was developed and showed good agreement with experimental results. In particular, the density distributions predicted by the FE simulation show very good agreement with the results obtained from optical densitometry. The springback model shows good results at pressures below 300 MPa, but at 500 MPa compaction pressure the springback results deviate considerably. This is mainly attributed to the lack of modeling the actual ejection procedure, and associated residual stress evolution, of the compact.

Conflict of Interests

The authors declare that there is no conflict of interests regarding the publication of this paper.

Acknowledgment

The authors would like to thank the Natural Science and Engineering Research Council (NSERC) of Canada for their financial support of this work.

References

[1] R. M. German, *Powder Metallurgy and Particulate Materials Processing: The Processes, Materials, Products, Properties, and Applications*, Metal Powder Industries Federation, Princeton, NJ, USA, 2005.

[2] M. D. Harding, I. W. Donaldson, R. L. Hexemer, M. A. Gharghouri, and D. P. Bishop, "Characterization of the microstructure, mechanical properties, and shot peening response of an industrially processed Al–Zn–Mg–Cu PM alloy," *Journal of Materials Processing Technology*, vol. 221, pp. 31–39, 2015.

[3] A. Ibrahim, D. P. Bishop, and G. J. Kipouros, "Sinterability and characterization of commercial aluminum powder metallurgy alloy Alumix 321," *Powder Technology*, vol. 279, pp. 106–112, 2015.

[4] M. M. Rahman, S. S. M. Nor, and H. Y. Rahman, "Investigation on the effect of lubrication and forming parameters to the green compact generated from iron powder through warm forming route," *Materials and Design*, vol. 32, no. 1, pp. 447–452, 2011.

[5] Z.-Y. Zhou, W.-B. Zhao, P.-Q. Chen, W.-P. Chen, M. Shao, and J.-W. Wang, "Simulation of die wall friction effect on density distribution in metallic powder compaction," *Transactions of Nonferrous Metals Society of China (English Edition)*, vol. 12, no. 5, pp. 890–893, 2002.

[6] T. L. Ngai, W.-P. Chen, Z.-Y. Xiao, L.-P. Wen, and Y.-B. Wu, "Die wall lubricated warm compaction of iron-based powder metallurgy material," *Transactions of Nonferrous Metals Society of China (English Edition)*, vol. 12, no. 6, pp. 1095–1098, 2002.

[7] Y. Y. Li, T. L. Ngai, D. T. Zhang, Y. Long, and W. Xia, "Effect of die wall lubrication on warm compaction powder metallurgy," in *Proceedings of the 10th International Manufacturing Conference in China (IMCC '02)*, pp. 354–358, Fujian, China, October 2002.

[8] J. D. Brown, G. S. P. Castle, F. Chagnon, and I. I. Inculet, "Electrostatic lubrication of moulds," in *Proceedings of the IEEE Industry Applications Conference, 32nd IAS Annual Meeting (IAS '97)*, vol. 3, pp. 1705–1709, IEEE, New Orleans, La, USA, October 1997.

[9] S. C. Lee and K. T. Kim, "Densification behavior of aluminum alloy powder under cold compaction," *International Journal of Mechanical Sciences*, vol. 44, no. 7, pp. 1295–1308, 2002.

[10] O. Coube and H. Riedel, "Numerical simulation of metal powder die compaction with special consideration of cracking," *Powder Metallurgy*, vol. 43, no. 2, pp. 123–131, 2000.

[11] G. Beck, S. Selig, D. A. Doman, and K. Plucknett, "Densitometry analysis to determine density distribution in green compacts," in *Proceedings of the International Conference on Powder Metallurgy & Particulate Materials*, San Francisco, Calif, USA, 2011.

[12] LSTC, *LS-DYNA Keyword User's Manual*, vol. 2, LSTC, Livermore, Calif, USA, 2014.

[13] L. Ma, T. Zahrah, and R. Fields, "Numerical three dimensional simulation of cold compaction and springback for prealloyed powder composites," *Powder Metallurgy*, vol. 47, no. 1, pp. 31–36, 2004.